Japanese Journal of Applied Physics
Vol. 47, No. 4, 2008, pp. 2005–2009

Molecular Dynamics of Diffusive-Ballistic Heat Conduction in Single-Walled Carbon Nanotubes

Junichiro SHIOMI and Shigeo MARUYAMA*

Department of Mechanical Engineering, The University of Tokyo, 7-3-1 Hongo, Bunkyo-ku, Tokyo 113-8656, Japan

(Received October 15, 2007; accepted December 18, 2007; published online April 18, 2008)

The diffusive-ballistic heat conduction of finite-length single-walled carbon nanotubes has been studied by means of nonequilibrium molecular dynamics simulations. The length dependence of thermal conductivity is quantified for a range of nanotube lengths up to 1.6 μm at room temperature. A gradual transition from nearly pure ballistic to diffusive-ballistic heat conduction was identified from the thermal conductivity profile. In the diffusive-ballistic regime, the profile exhibits power-law length dependence and does not converge even for a tube length of 1.6 μm. Furthermore, the diameter dependence of thermal conductivity suggests considerable suppression of the diffusion effect as the diameter decreases.
[DOI: 10.1143/JJAP.47.2005]

KEYWORDS: carbon nanotube, molecular dynamics, thermal conductivity, phonon transport

1. Introduction

The expanding roles expected for single-walled carbon nanotubes (SWNTs) include applications for various electrical and thermal devices due to their unique properties.[1)] SWNTs are thought to possess high thermal conductivity due to their strong carbon bonds and the quasi-one-dimensional structure.[2)] On considering the actual applications, one of the essential tasks is to characterize the thermal properties of SWNTs not only for thermal devices but also for electrical devices since they determine the affordable amount of electrical current that can pass through the system.

Following the thermal conductivity measurements of SWNTs in the form of mats and bundles,[3)] with the advances in SWNT synthesis and micro electro mechanical systems (MEMS) techniques, the thermal conductivity (or thermal conductance) measurements of individual carbon nanotubes have been recently reported not only for multi-walled carbon nanotubes,[4,5)] but also for SWNTs.[6,7)] However, the thermal property measurements of SWNTs in experiments are still extremely challenging as there are potential uncertainties due to various technicalities, for instance related to the contact resistances between thermal reservoirs and an SWNT. Uncertainties also arise in the identification of an isolated SWNT and its diameter. Therefore, reliable theories and numerical simulations are greatly demanded, particularly to investigate detailed heat conduction characteristics that are not yet accessible in experiments. One such heat conduction characteristic with practical importance is the size effect on thermal conductivity. In general, a size dependence of thermal conductivity appears when the system characteristic length is smaller or comparable to the phonon mean free path.[8)] For SWNTs, because of the expected long phonon mean free path, the regime of the length effect stretches beyond their realistic length in many applications. The length effect has been demonstrated using molecular dynamics (MD) simulations[9,10)] and the power-law divergence has been discussed with analogy to the low-dimensional models, where the *hydrodynamic effect* gives rise to the long-time heat flux correlation.[11)] More recently, the length dependence of thermal conductivity was investigated up to fully diffusive phonon transport regime using a kinetic approach,[12)] where the divergence due to long-wavelength phonons was shown to disappear in the presence of second-order (or higher) three-phonon scattering processes. The transition from pure ballistic to diffusive-ballistic phonon transport has been discussed by modeling the energy transmission based on the ratio of the overall average phonon mean free path to L.[13)]

In this paper, we aim to demonstrate the diffusive-ballistic transition of heat conduction in SWNTs at room temperature by calculating the thermal conductivity for a range of lengths using nonequilibrium classical MD simulations. MD simulations are capable of handling the phonon transport of all the phonon branches, unlike the kinetic approach with relaxation approximations.[12)] As shown later, this capability is important for relatively short SWNTs with significant ballistic phonon transport, particularly at room temperature, where a wide range of phonon branches are populated.

2. Molecular Dynamics Model

The carbon–carbon interactions were modeled using the Brenner potential[14)] in a simplified form,[15)] where the total potential energy of the system is expressed as

$$E = \sum_i \sum_{j(i<j)} \lfloor V_{\mathrm{R}}(r_{ij}) - B^*_{ij} V_{\mathrm{A}}(r_{ij}) \rfloor. \quad (1)$$

Here, $V_{\mathrm{R}}(r)$ and $V_{\mathrm{A}}(r)$ are the repulsive and attractive force terms, respectively, which take a Morse-type form with a certain cutoff function. B^*_{ij} represents the effect of the bonding order parameters. For the potential parameters, we employ a set that has been shown to reproduce the linear phonon transport properties with sufficient accuracy.[9,10)] The velocity Verlet method was adopted to integrate the equation of motion with a time step of 0.5 fs. The suitability of the classical approach is indicated by the expected dominant contribution to the heat conduction from phonons compared with that from electrons.[16,17)]

When simulating ballistic phonon transport using MD simulations, the linear transport properties (group velocity) need to be reproduced with sufficient accuracy. This needs to

*E-mail address: maruyama@photon.t.u-tokyo.ac.jp

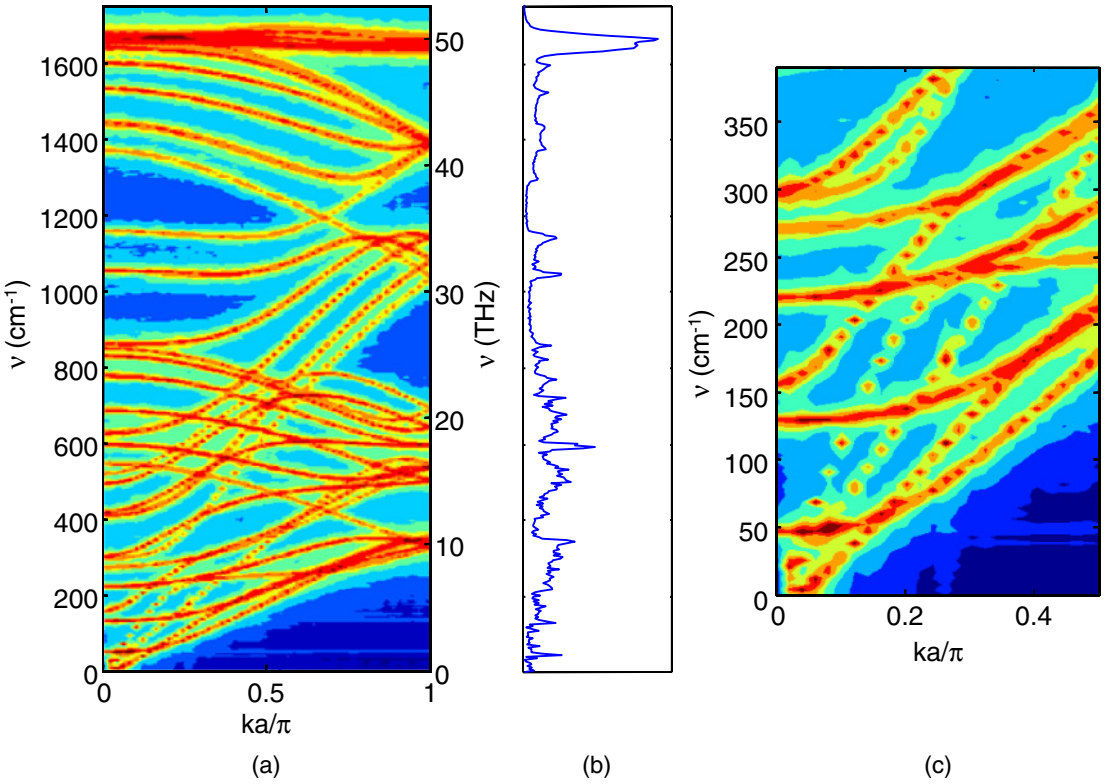

Fig. 1. (Color online) (a) Discrete phonon dispersion relations and (b) phonon DOS of a 25-nm-long (5,5) SWNT. The dispersion relations were obtained by computing the phonon energy spectral density from MD simulations.[18] The wave vector k-space is normalized by the Brillouin zone width, π/a. In the current case with an armchair SWNT, $a = \sqrt{3}A_{c\text{–}c}$, where $A_{c\text{–}c}$ is the interatomic distance. The focused view (c) shows the phonon dispersion in the low-frequency region for clarity.

be satisfied for phonons with a wide range of frequencies as their ballistic transport becomes important for short SWNTs at room temperature. The linear phonon transport properties can be visualized by the dispersion relations, which can be computed from MD simulations by obtaining the two-dimensional Fourier spectra of the time history of the velocity field along an SWNT. In Fig. 1, the spectra of a 25 nm (5,5) SWNT at 300 K with a periodic boundary condition is presented together with the corresponding phonon density of states (DOS). The phonon energy spectral density is computed as[18]

$$\Phi(\omega,k) = \frac{m}{2}\sum_{\alpha}^{p}\sum^{3}\left|\frac{1}{N}\sum_{n=0}^{N-1}\left[\exp\left(i\frac{n}{N}k\right)\int v_\alpha(n,t)\exp(-i\omega t)\,dt\right]\right|^2 \quad (\alpha = r,\phi,z), \tag{2}$$

where N is the number of atoms in the longitudinal (z) direction (the number of unit cells in the nanotube). p and m are the number of atoms per unit cell and the mass of a carbon atom, respectively. The data are discrete due to the finite length of the nanotube, and the broadening of the spectral peaks indicates the thermal phonon scattering. The overall feature of the dispersion relations obtained from MD simulations agrees with the reported theoretical models,[1,19] and particularly well with the mechanical model of Mahan and Jeon.[19] The phonon DOS $g(\omega)$ can be calculated from

$$g(\omega)\hbar\omega\eta(\omega) = \sum_k \Phi(\omega,k),$$

where the equilibrium phonon distribution is $\eta(\omega) = k_B T/\hbar\omega$ at the classical limit.

Note that for SWNTs, as the number of phonon branches is determined by the number of atoms in a unit cell, even for armchair (or zigzag) SWNTs whose unit cells contain fewer atoms than other structures with similar diameters, the dispersion relation depicts diverse phonon branches, as shown in Fig. 1 for a (5,5) SWNT. There are optical phonon modes with a small circumferential wave number and low frequency that have similar dispersion characteristics and heat capacity to the acoustic modes, particularly in the intermediate-wave-vector (k) regime. Although, acoustic modes may still possess the longest mean free path, the contribution of these optical modes is expected to become important when their mean free paths are comparable to L.

3. Thermal Conductivity Calculations

The thermal conductivity λ of an SWNT was measured by nonequilibrium MD simulations. After reaching an isothermal state at 300 K by auxiliary velocity scaling control, the temperature-controlled layers on both ends of the SWNT were activated to apply a temperature difference of 20 K. Eventually the system converged to a quasi-stationary state with a linear temperature gradient. The simulation time ranges within 3–18 ns because the data convergence time

depends on the system size. By calculating the heat flux along the SWNT from the energy budgets of the thermostats, λ was calculated through Fourier's law. The cross-sectional area A of an SWNT was defined using a ring of van der Waals thickness πbd, where $b = 0.34$ nm. The validity of the temperature gradient of 20 K for short SWNTs was examined by performing additional simulations for a temperature gradient of 10 K in the case of $L = 25$ nm. The converged value of thermal conductivity was 236 W/mK compared with 223 W/mK for the 20 K gradient case. Hence, the difference was confirmed to be small enough. The validity of using thermal conductivity to express the heat conduction of the current system is questionable due to the extensive ballistic heat transport. Furthermore, the definition of the area of an isolated SWNT is rather ambiguous. Although simply expressing the heat conduction as thermal conductance may be more suitable, here we use thermal conductivity for the sake of comparison with previous studies.

Upon carrying out nonequilibrium MD simulations by locally applying thermostats to a crystal system, the interface between the temperature-controlled part and the rest of the system typically gives rise to a thermal boundary resistance (TBR). A TBR appears due to the mismatching of the lattice-vibrational spectra of the temperature-controlled part and the rest of the system. This mismatching causes the reflection of phonons and alters the scattering dynamics at the interface. Since a TBR is expected to influence the local nonequilibrium phonon distribution and hence alter the heat conduction, thermostats and their parameters need to be carefully selected to minimize the TBR.

It is important to state that the TBR effect is not entirely a numerical artifact. For instance, in practical use of the lateral heat conduction of SWNTs to promote heat transfer, finite-length SWNTs would be bounded by connections to other materials. In this case, the heat conduction properties would be inevitably altered by TBRs at the connections. Therefore, in fact, it would be more realistic to examine the heat conduction of SWNTs with presence of such interfacial thermal resistances, although the formulation of a general case would be difficult since such effects would be strongly case-dependent. In the current study, for the sake of comparison with other reported theoretical works and to focus on studying the intrinsic dynamics, we aim to construct an ideal case by minimizing the TBR effect.

Firstly, the temperature gradient was applied using the phantom technique as in the previous works.[9,10] Here, a phantom thermostat consists of a fixed layer and a phantom layer, which are both monolayer unit cells. The phantom layer is placed between the fixed layer at the tube end and the rest of the SWNT, and is controlled by the Langevin equation. The Debye temperature of diamond was chosen as the damping parameter of the Langevin equation. This formulation aims to damp the phonons traveling into the phantom layer and hence to prevent the phonons from being reflected at the tube ends. Therefore, a phantom thermostat ideally models isothermal layers with sufficient length.

For SWNTs, the simulations using the phantom technique were validated by performing an additional set of simulations adopting standard Nose–Hoover (NH) thermostats.[20,21] A straightforward application of an NH thermostat without any virtual dynamics makes the method simple and robust, although it is more computationally expensive than the previous method. The thermostats have two tuning parameters; the length of the temperature-controlled part L_c and the relaxation time τ. Figure 2 shows the temperature profiles obtained by using the NH thermostat for various values of L_c, where distinct TBRs can be observed as temperature jumps. For instance, in the case of $L_c = 0.01L$, temperature jumps at the interfaces account for about 50% of the total temperature difference between the tube ends.

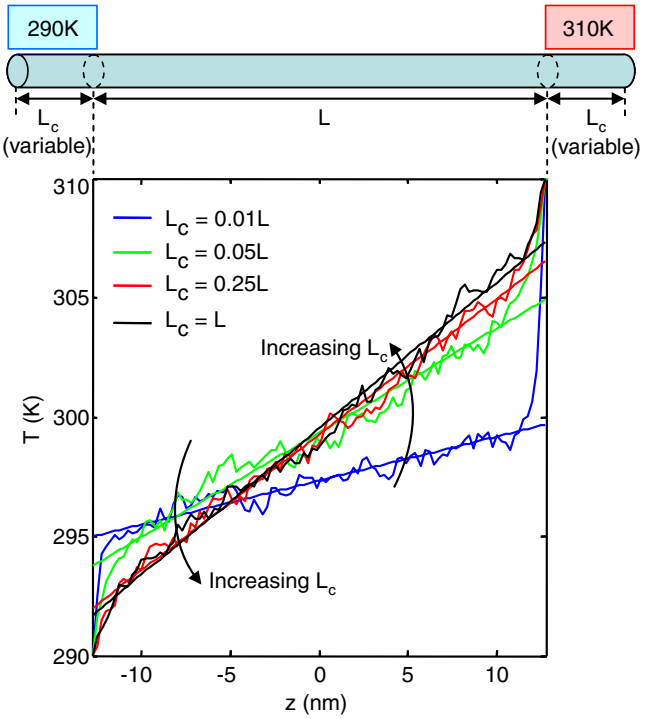

Fig. 2. (Color online) Influence of the length of the layers controlled by NH thermostat (L_c) on the temperature profile ($L = 25$ nm).

In order to minimize the TBRs, parameters L_c and τ were tuned. The influences of L_c and τ on the key thermal properties are shown in Figs. 2–4. The elongation of L_c permits longer-wavelength phonon modes and hence attenuates the discrepancy of the phonon spectra between the temperature-controlled part and the rest of the nanotube. This can be seen in the L_c dependence of temperature profiles (Fig. 2), where a shorter L_c results in larger TBRs. More detailed views are given in Figs. 3(a)–3(c) which show the L_c dependences of the temperature gradient, heat flux, and thermal conductivity, respectively. Both the temperature gradient and the heat flux increased with L_c and eventually saturated at the upper limit $L_c/L \sim 1$, independently of τ. The corresponding trend of λ is similar except for the value for $L_c/L = 0.01$. Therefore, considering the computational cost, we used $L_c = 0.5L$ as an optimal value.

Regarding the relaxation time, a longer τ is expected to give the temperature-controlled layers more time to adjust the spectrum to that of the rest of the SWNT. The variation of TBRs with respect to τ is shown in Fig. 4 for $L_c = 0.5L$. The figure shows the sum of the TBRs on the hot and cold sides R for various nanotube lengths, within the parameter bounds ($40 < \tau < 4$ ns), beyond which the quasi-linear temperature profile is significantly disturbed. Below the

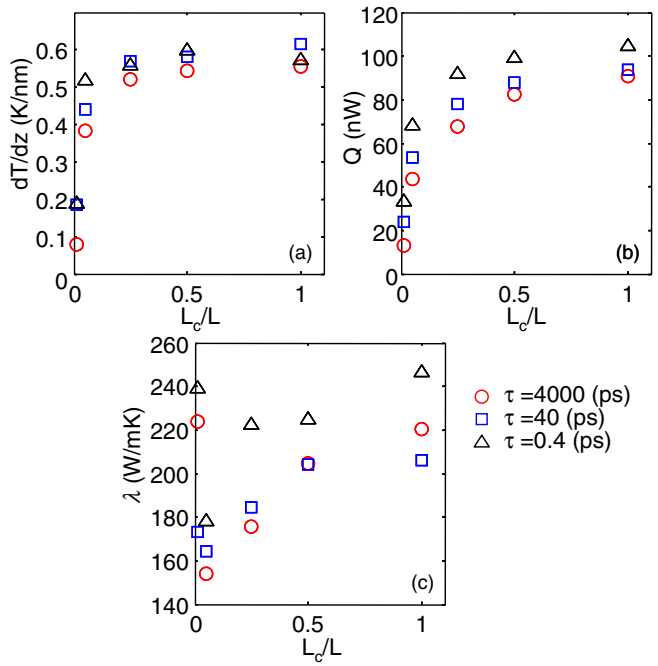

Fig. 3. (Color online) Influence of L_c/L and relaxation time of NH thermostat on (a) the axial temperature gradient dT/dz, (b) heat flux through the system Q, and (c) thermal conductivity λ. $L = 25$ nm.

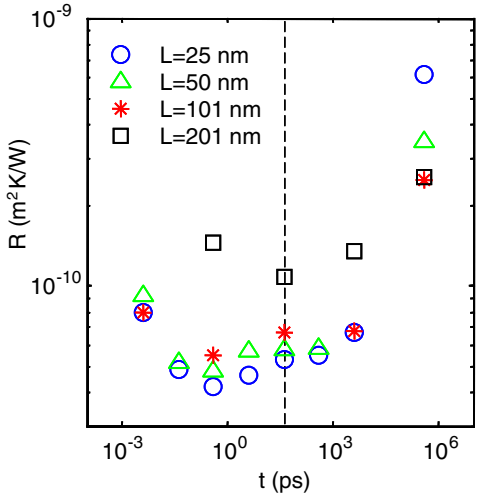

Fig. 4. (Color online) Influence of the relaxation time of NH thermostat on the sum of TBRs on the hot and cold sides of SWNT for different values of L ($L_c = 0.5L$). The dashed line shows $\tau = 40$ ps.

lower bound, the phonon spectra of the temperature-controlled layers and the rest of the SWNT were found to exhibit severe mismatching. On the other hand, above the upper bound, the data hardly converged. The figure shows that R takes a minimum value for a critical relaxation time τ_{cr}. On varying L from 25 to 201 nm, τ_{cr} exhibits a moderate variation between 400 fs and 40 ps. On considering the observed trend that τ_{cr} increases with L, we take $\tau = 40$ ps as the optimal value. Note that one order difference in τ results in approximately 10% difference in thermal conductivity.

4. Effects of Length and Diameter on SWNT Thermal Conductivity

Figure 5 shows the length effect on the thermal conductivity of SWNTs for a range of L up to 1.6 μm. It can be seen that the differences between the values obtained for (5, 5) SWNTs using the phantom technique (filled circles) and NH thermostats (open circles) are negligible. The overall trend of the slope ($\partial\lambda/\partial L$) clearly indicates the gradual transition from strongly ballistic to diffusive-ballistic phonon transport. When all the phonons experience ballistic phonon transport, λ is proportional to L (constant thermal conductance). The asymptotic match of the gradients of the thermal conductivity profiles to that of the dashed line suggests dominant ballistic phonon transport at the small L limits. Note that on considering the significant phonon population in a range of phonon branches at room temperature, we expect contributions to the heat conduction not only from the ballistic transport of acoustic phonon modes but also from that of various optical phonon modes in the small-L regime. This is consistent with the results of the MD realization of non-Fourier heat conduction in 25 nm long SWNTs, where the ballistic transport of collective optical phonons was observed to play an important role.[18] The gradient $\partial\lambda/\partial L$ gradually decreases as L increases since the phonon mean free paths gradually become shorter relative to L, i.e., diffusive phonon transport is gradually enhanced with respect to ballistic phonon transport. The figure also shows that the thermal conductivity of SWNTs does not converge in the range of L explored in the current work ($\leq$1.6 μm). Furthermore, in connection with the discussion on the divergence of thermal conductivity,[11,12] we could fit power-law functions to the obtained profiles. As denoted in Fig. 5, by fitting power laws for $L > 100$ nm, we obtained the exponents of 0.19 and 0.33 for (5, 5) and (3, 3) SWNTs, respectively. The power-law length dependence of thermal conductivity can be explained by the weak three-phonon scattering of long-wavelength phonons compromised by the higher order processes[12] and/or the long-time heat current correlations in low dimensions.[22]

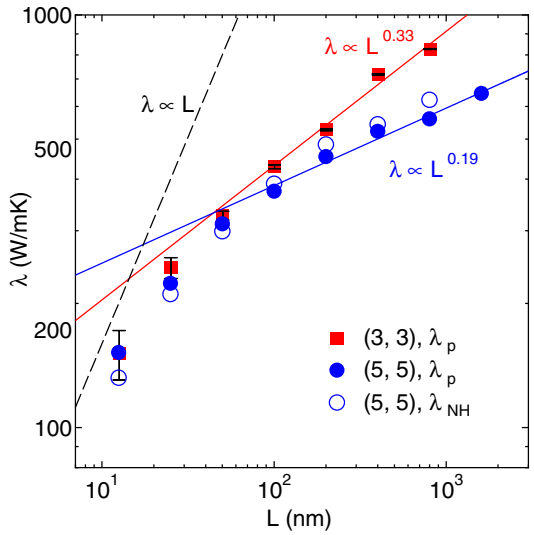

Fig. 5. (Color online) Length dependences of SWNT thermal conductivity for two different diameters. λ_p and λ_{NH} denote the values obtained by using phantom and NH thermostats, respectively. The error bars are based on the fitting residuals in the thermal conductivity calculations. The residuals were largest in the case of (3, 3) SWNTs. The thermal conductivity profiles of (3, 3) and (5, 5) SWNTs for $L > 100$ nm were fitted to power laws. The dashed line shows $\lambda \propto L$ with an arbitrary slope.

Let us now examine the diameter (d) dependence of SWNT thermal conductivity. For small L, where the phonon transport is dominantly ballistic, the thermal conductivity exhibits negligible dependence on the diameter. This independence for small L is consistent with the above discussion that ballistic phonon transport is dominant in this regime. At the ballistic phonon transport limit, where all the populated phonons experience ballistic transport, thermal conductance is proportional to the number of atoms per unit cell, i.e., the diameter, if we ignore the variation of the linear phonon transport property (dispersion relations) due to the changes in the unit-cell size and the curvature. This means, with the current definition of $A = \pi bd$, that the thermal conductivity is independent of the diameter. As L increases, the diameter dependence becomes noticeable, and the thermal conductivity profiles of $(3, 3)$ and $(5, 5)$ SWNTs deviate from each other above $L \sim 100\,\mathrm{nm}$. Current results show that, in the large-L regime, thermal conductivity is greater, i.e., the diffusion effect is smaller for SWNTs with smaller d. The trend is consistent with the above-mentioned possible origins of the power-law length dependence. The exponent of the thermal conductivity divergence due to the long-wavelength phonons increases as d decreases[13] because of the variation in the phonon DOS. Similarly, the long-time correlation[22] is also expected to increase as d decreases due to the reduction of the number of phonon channels per length. The exact mechanism of the power-law length dependence cannot be identified from the present diameter dependence of the exponent. A detailed examination of the heat flux autocorrelation function in the equilibrium framework is needed to discuss this mechanism further.

5. Conclusions

Nonequilibrium MD simulations were conducted to investigate the heat conduction of SWNTs at room temperature. The effects of the length and diameter on the thermal conductivity were quantified over a range of L and for two different diameters. A gradual transition from nearly pure ballistic phonon transport to diffusive-ballistic phonon transport was clearly observed. In the small-L regime with strong ballistic transport, there is a significant contribution to the heat conduction from a range of optical phonons. A consistent picture of ballistic phonon transport was obtained from the diameter dependence; thermal conductivity is diameter-invariant for small L. In the regime of L with significant diffusive phonon transport, power-law length dependence was identified with increasing exponent as the diameter decreased. In this regime, the thermal conductivity does not converge even for $1.6\,\mu\mathrm{m}$ tube length.

Acknowledgements

This work is supported in part by Grants-in-Aid for Scientific Research 19206024, 19054003, 19051016, and 19860022.

1) R. Saito, G. Dresselhaus, and M. S. Dresselhaus: *Physical Properties of Carbon Nanotubes* (Imperial College Press, London, 1998).
2) S. Berber, Y.-K. Kwon, and D. Tomanek: Phys. Rev. Lett. **84** (2000) 4613.
3) J. Hone, M. C. Llaguno, M. J. Biercuk, A. T. Johnson, B. Batlogg, Z. Benes, and J. E. Fischer: Appl. Phys. A **74** (2002) 339.
4) P. Kim, L. Shi, A. Majumdar, and P. L. McEuen: Phys. Rev. Lett. **87** (2001) 215502.
5) M. Fujii, X. Zhang, H. Xie, H. Ago, K. Takahashi, T. Ikuta, H. Abe, and T. Shimizu: Phys. Rev. Lett. **95** (2005) 065502.
6) C. Yu, L. Shi, Z. Yao, D. Li, and A. Majumdar: Nano Lett. **5** (2005) 1842.
7) E. Pop, D. Mann, Q. Wang, K. Goodson, and H. Dai: Nano Lett. **6** (2006) 96.
8) G. Chen: *Nanoscale Energy Transport and Conversion* (Oxford University Press, New York, 2005).
9) S. Maruyama: Physica B **323** (2002) 193.
10) S. Maruyama: Nanoscale Microscale Thermophys. Eng. **7** (2003) 41.
11) R. Livi and S. Lepri: Nature **421** (2003) 327.
12) N. Mingo and D. A. Broido: Nano Lett. **5** (2005) 1221.
13) J. Wang and J.-S. Wang: Appl. Phys. Lett. **88** (2006) 111909.
14) D. W. Brenner: Phys. Rev. B **42** (1990) 9458.
15) Y. Yamaguchi and S. Maruyama: Chem. Phys. Lett. **286** (1998) 336.
16) J. Hone, M. Whitney, C. Piskoti, and A. Zettl: Phys. Rev. B **59** (1999) R2514.
17) T. Yamamoto, S. Watanabe, and K. Watanabe: Phys. Rev. Lett. **92** (2004) 075502.
18) J. Shiomi and S. Maruyama: Phys. Rev. B **73** (2006) 205420.
19) G. D. Mahan and G. S. Jeon: Phys. Rev. B **70** (2004) 075405.
20) S. Nose: J. Chem. Phys. **81** (1984) 511.
21) W. G. Hoover: Phys. Rev. A **31** (1985) 1695.
22) S. Lepri, R. Livi, and A. Politi: Phys. Rep. **377** (2003) 1.